



Weak limit of the three-state quantum walk on the line

Stefan Falkner and Stefan Boettcher

Department of Physics, Emory University, Atlanta, Georgia 30322, USA

(Received 20 May 2014; published 8 July 2014)

We revisit the one-dimensional discrete time quantum walk with three states and the Grover coin, the simplest model that exhibits localization in a quantum walk. We derive analytic expressions for the localization and a long-time approximation for the entire probability density function (PDF). We find the possibility for asymmetric localization to the extreme that it vanishes completely on one site of the initial conditions. We also connect the time-averaged approximation of the PDF found by Inui *et al.* [*Phys. Rev. E* **72**, 056112 (2005)] to a spatial average of the walk. We show that this smoothed approximation predicts moments of the real PDF accurately.

DOI: [10.1103/PhysRevA.90.012307](https://doi.org/10.1103/PhysRevA.90.012307)

PACS number(s): 03.67.Ac, 05.10.Cc, 05.40.Fb

I. INTRODUCTION

Quantum walks have been the subject of research for the past 20 years [1–4]. They were originally proposed as a description for quantum transport in a one-dimensional system [5,6]. However, quantum walks soon received considerable prominence as the driving dynamics behind quantum search algorithms [7,8], leading to many systematic studies of their asymptotic properties [9–12]. Other applications, such as to the graph isomorphism problem [13,14], further increased the interest. The realization of their capability for general quantum computations [15,16] suggests that understanding quantum walks is a quest for a better understanding of quantum computing itself.

Due to its wealth of possible parameters, the discrete time quantum walk has been studied extensively. From the basic properties of the simplest possible quantum walk on the one-dimensional line [10], time-dependent coins [17] and site-dependent coins [18] are only some of the many extensions that have been investigated. For a more comprehensive review, we refer the reader to [3] and the references within.

In this paper, we revisit the one-dimensional quantum walk with the three-dimensional Grover coin, previously considered by Inui *et al.* [19]. They discussed a variation of the walk on the line, where the walker can remain on the site during a time step, and found interesting differences from the case of a two-dimensional coin. Most notably, there is a finite probability that the quantum walk strongly localizes around the initial site, as previously found on square lattices [20]. In fact, this model is the simplest model exhibiting localization, a distinctly quantum effect entirely absent in the corresponding classical random walks. A thorough understanding of localization in this simple context becomes particularly relevant in light of the fact that this phenomenon is commonplace in higher-dimensional systems [3]. Furthermore, in systems without translational invariance, for instance, localization might be asymptotically complete and broadly distributed [21].

Here, we extend the findings of [19] by analytic expressions for the localization, calculate the weak limit of the probability density function (PDF), and show its equivalence to a spatial average over a local neighborhood. We provide explicit expressions for general initial conditions present on one site, study the convergence, and compare our analytic predictions for moments with those from numerical simulations.

The paper is organized as follows. In Sec. II, we review the basics for the three-state quantum walk on the line.

In Sec. III we show how the long-time behavior can be obtained, with an accurate description of the localization and an approximation for the spreading front. In Sec. IV, we introduce an approximation that leads to a smoothed PDF, corresponding to a spatial as well as temporal average. Finally, in Sec. V, we summarize our findings.

II. THE THREE-STATE QUANTUM WALK

In the common description of the discrete time quantum walk, every time step consists of two parts. First, the coin (operator) is applied to the internal degree of freedom (coin state) at every site. This is followed by the shift operator, translating components of the coin state to neighboring sites. Here, we study the case of the one-dimensional quantum walk with a three-dimensional coin space, driven by the Grover coin:

$$C = \frac{1}{3} \begin{bmatrix} -1 & 2 & 2 \\ 2 & -1 & 2 \\ 2 & 2 & -1 \end{bmatrix}. \quad (1)$$

Our convention for the shift operation is the following: the first component is moved to the left, the third component is moved to the right, while the second one remains on the site. The matrices \mathcal{P} , \mathcal{Q} , and \mathcal{R} (see Fig. 1) combine both steps into a single operation, leading to the master equation describing the time evolution at any site n :

$$|\psi_n^{t+1}\rangle = \mathcal{P} |\psi_{n-1}^t\rangle + \mathcal{Q} |\psi_{n+1}^t\rangle + \mathcal{R} |\psi_n^t\rangle, \quad (2)$$

with

$$\mathcal{P} = \begin{bmatrix} 0 & 0 & 0 \\ 0 & 0 & 0 \\ \frac{2}{3} & \frac{2}{3} & -\frac{1}{3} \end{bmatrix}, \quad \mathcal{Q} = \begin{bmatrix} -\frac{1}{3} & \frac{2}{3} & \frac{2}{3} \\ 0 & 0 & 0 \\ 0 & 0 & 0 \end{bmatrix},$$

$$\mathcal{R} = \begin{bmatrix} 0 & 0 & 0 \\ \frac{2}{3} & -\frac{1}{3} & \frac{2}{3} \\ 0 & 0 & 0 \end{bmatrix}.$$

For simplicity, we assume the initial conditions are only nonzero on site $n = 0$, i.e.,

$$|\psi_n^0\rangle = \delta_{n,0} |\psi_0^0\rangle. \quad (3)$$

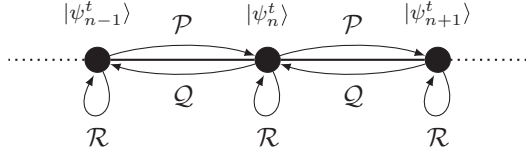


FIG. 1. The one-dimensional quantum walk with a three-dimensional coin. The matrices \mathcal{P} , \mathcal{Q} , and \mathcal{R} facilitate a right hop, a left hop, or no change in position, respectively.

These equations can be solved by a Fourier transform:

$$|\tilde{\psi}^t\rangle = \sum_{n=-\infty}^{\infty} e^{-ikn} |\psi_n^t\rangle. \quad (4)$$

From here on, a tilde indicates quantities with a k dependence, which we will not explicitly show. Applying Eq. (4) to Eq. (2) yields the master equation in Fourier space:

$$|\tilde{\psi}^{t+1}\rangle = \frac{1}{3} \underbrace{\begin{bmatrix} -\kappa & 2\kappa & 2\kappa \\ 2 & -1 & 2 \\ 2\kappa^{-1} & 2\kappa^{-1} & -\kappa^{-1} \end{bmatrix}}_{:=\tilde{\mathcal{C}}} \cdot |\tilde{\psi}^t\rangle, \quad (5)$$

where $\kappa = e^{ik}$. The solution to this equation,

$$|\tilde{\psi}^t\rangle = \tilde{\mathcal{C}}^t |\psi_0^0\rangle, \quad (6)$$

can be found by computing the eigenvalue decomposition:

$$\mathcal{T}^{-1} \tilde{\mathcal{C}} \mathcal{T} = \begin{bmatrix} \tilde{\lambda}_1 & 0 & 0 \\ 0 & \tilde{\lambda}_2 & 0 \\ 0 & 0 & \tilde{\lambda}_3 \end{bmatrix}. \quad (7)$$

One eigenvalue is purely real, $\tilde{\lambda}_1 = 1$, whereas the other two obey

$$\lambda_{2,3} = e^{\pm i\tilde{\omega}} \quad \text{and} \quad \cos(\tilde{\omega}) = -\frac{2}{3} - \frac{\cos(k)}{3}. \quad (8)$$

The t th power of $\tilde{\mathcal{C}}$ can then be expressed as

$$\tilde{\mathcal{C}}^t = \tilde{\mathcal{M}}_1 + \tilde{\lambda}_2^t \tilde{\mathcal{M}}_2 + \tilde{\lambda}_3^t \tilde{\mathcal{M}}_3. \quad (9)$$

A representation of \mathcal{T} and the $\tilde{\mathcal{M}}$ matrices can be found in the supplementary Mathematica notebook [22]. In the end, the real space solution is obtained by performing the inverse Fourier transform:

$$|\psi_n^t\rangle = \frac{1}{2\pi} \int_{-\pi}^{\pi} e^{ink} |\tilde{\psi}^t\rangle dk. \quad (10)$$

In the next section, we perform an asymptotic approximation in the long-time limit to find the leading behavior of the PDF.

III. LONG-TIME APPROXIMATION

In this section, we evaluate Eq. (10) in the limit of $t \rightarrow \infty$. First, we compute the time-independent part of $|\psi_n^t\rangle$ that manifests itself as localization. As a test, we compare our result with numerical simulations. Afterward, we use the method of stationary phase to find an approximation for the remaining, time-dependent part.

A. The stationary distribution

One can see from Eq. (9) that a time-independent component of $|\tilde{\psi}^t\rangle$ can exist due to the constant eigenvalue of $\tilde{\mathcal{C}}$. The inverse Fourier transform of this part can be computed exactly by employing the residue theorem. Note that the corresponding integral for this part following from Eqs. (9) and (10), in terms of κ , reads

$$|\psi_n^\infty\rangle = \frac{1}{2\pi i} \underbrace{\oint_{|\kappa|=1} \kappa^{n-1} \tilde{\mathcal{M}}_1 d\kappa}_{:=\mathcal{U}_1(n)} |\psi_0^0\rangle. \quad (11)$$

The details of this calculation can be found in Appendix A, but the essential observation is that all components of $\tilde{\mathcal{M}}_1$ share the same poles,

$$\kappa_{\pm} = -5 \pm 2\sqrt{6}, \quad (12)$$

of which only κ_+ is inside the unit circle. For $n \leq 0$, there is an additional pole at $\kappa = 0$. By straightforward calculations, we find an expression for $\mathcal{U}_1(n)$ for different regimes for n :

$$\begin{aligned} \mathcal{U}_1(n < 0) &= \frac{\kappa_-^n}{\sqrt{6}} \begin{bmatrix} 1 & -2 - \sqrt{6} & -5 - 2\sqrt{6} \\ -2 + \sqrt{6} & -2 & -2 - \sqrt{6} \\ -5 + 2\sqrt{6} & -2 + \sqrt{6} & 1 \end{bmatrix}, \\ \mathcal{U}_1(n = 0) &= \frac{1}{\sqrt{6}} \begin{bmatrix} 1 & -2 + \sqrt{6} & -5 + 2\sqrt{6} \\ -2 + \sqrt{6} & -2 + \sqrt{6} & -2 + \sqrt{6} \\ -5 + 2\sqrt{6} & -2 + \sqrt{6} & 1 \end{bmatrix}, \\ \mathcal{U}_1(n > 0) &= \frac{\kappa_+^n}{\sqrt{6}} \begin{bmatrix} 1 & -2 + \sqrt{6} & -5 + 2\sqrt{6} \\ -2 - \sqrt{6} & -2 & -2 + \sqrt{6} \\ -5 - 2\sqrt{6} & -2 - \sqrt{6} & 1 \end{bmatrix}. \end{aligned} \quad (13)$$

At first, the case distinction in the sign of n seems counterintuitive, but the comparison to the numerics in Fig. 2 reveals the possibility of an asymmetric localization around the initial site.

To obtain the stationary PDF, we calculate

$$p_1(n) = \langle \psi_n^\infty | \psi_n^\infty \rangle = \langle \psi_0^0 | U_1^\dagger(n) U_1(n) | \psi_0^0 \rangle. \quad (14)$$

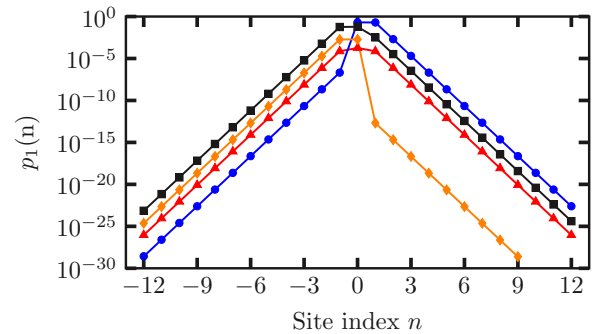


FIG. 2. (Color online) Comparison between analytic prediction (lines) and numerical simulation after $T = 2^{20}$ time steps (symbols) for the localization around $n = 0$. The initial conditions are $|\psi_0^0\rangle \propto (1, -1.9, 1)$ (red triangles), $|\psi_0^0\rangle \propto (10, 0, 1)$ (blue circles), $|\psi_0^0\rangle \propto (1, -3, 2 + i)$ (black squares), and $|\psi_0^0\rangle \propto (410, -800, 499)$ (orange diamonds). They have been chosen to show the possible asymmetry of $p_1(n)$.

For general initial conditions, $p_1(n)$ still contains the case distinction in n , but the localization only at the initial site for arbitrary $|\psi_0^0\rangle = (\alpha, \beta, \gamma)^T$, for example, reads

$$(\bar{\alpha}, \bar{\beta}, \bar{\gamma}) \mathcal{U}_1^\dagger(0) \mathcal{U}_1(0) \cdot \begin{pmatrix} \alpha \\ \beta \\ \gamma \end{pmatrix} = (5 - 2\sqrt{6})[(2\alpha + \beta)\bar{\alpha} \\ + (\alpha + \beta + \gamma)\bar{\beta} + (\beta + 2\gamma)\bar{\gamma}], \quad (15)$$

which coincides with the result in [19].

We point out that the stationary PDF always decays exponentially away from the initial site as $p_1(n) \sim \kappa_+^{2|n|}$ independent of the initial conditions, even though the proportionality constant might differ from positive to negative n . The initial conditions $|\psi_0^0\rangle \propto (1, -2, 1)$ comprise a non-generic case where the localization *completely vanishes*. There exists also a whole family, $|\psi_0^0\rangle \propto (-a(1 + \kappa_\pm)/2 - b\kappa_\pm, a, b)$ with $a, b \in \mathbb{R}$, where the localization vanishes for positive (negative) n while still exponentially decaying for negative (positive) values.

To show that our calculations describe the localized part comprehensively, we compare to a long simulation of a system, where the system is large enough that the finite size has no influence on the PDF near the initial site at the end of the simulation. The system starts with different initial conditions and evolves for 2^{20} time steps. In the end, the final probabilities at sites around the origin are recorded. Figure 2 shows the comparison between evaluating Eq. (14) and the simulation. To demonstrate the asymmetry, we choose four particular initial conditions.

The rapid decay renders estimating $p_1(n)$ with simulations for $|n| \gg 10$ problematic. The values range over 30 orders of magnitude, challenging the machine precision used in the simulations. Furthermore, the time to converge to $p_1(n)$ grows exponentially with n , as we will see, which restricts the numerical evaluation, as system size would have to grow exponentially as well. The case of zero localization for either $n > 0$ or $n < 0$ is also hard to resolve numerically due to the limited machine precision, but the blue and orange curves in Fig. 2 demonstrate the asymmetry, and the jump at $n = 0$ can be arbitrarily steep.

B. Approximating the time-dependent integrals

After solving the time-independent part analytically, we have to resort to approximations for the time-dependent part of $|\tilde{\psi}^t\rangle$ in the limit $t \rightarrow \infty$. In analogy to Eq. (11), we define

$$\mathcal{U}_{2,3}(t, n) = \frac{1}{2\pi} \int_{-\pi}^{\pi} e^{ikn} \tilde{\mathcal{M}}_{2,3} \tilde{\lambda}_{2,3}^t dk, \quad (16)$$

such that the sum $\mathcal{U}_1 + \mathcal{U}_2 + \mathcal{U}_3 = \tilde{\mathcal{C}}^t$ expresses the full time evolution. By introducing the “velocity” v via

$$n = vt \quad (17)$$

and using Eq. (8), we write the integrals as

$$\frac{1}{2\pi} \int_{-\pi}^{\pi} \tilde{f}(k) e^{it(vk \pm \tilde{\omega})} dk,$$

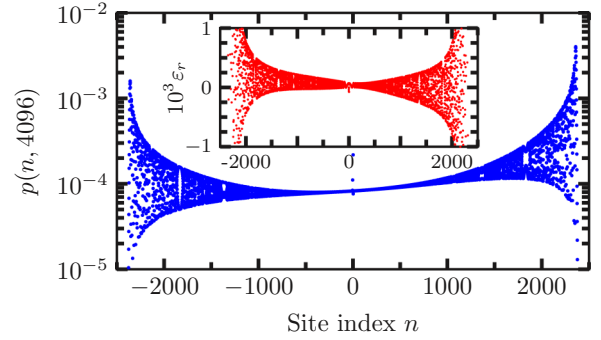


FIG. 3. (Color online) The PDF of the walk (blue dots) after $t = 4096$ steps with the initial conditions $|\psi_0^0\rangle \propto (0, i, 1)$. Beyond the shown index range, the probability is essentially zero. Inset: Relative difference between the asymptotic approximation and the numerical values. The prediction is fairly good for a wide range of points.

where the function \tilde{f} represents the different (slowly varying) elements of the $\tilde{\mathcal{M}}$ matrices.

This form is known as a generalized Fourier integral [23], and the leading long-time behavior can be found by the method of stationary phase. The method assumes that the main contribution to the integral stems from a small region of k around an extremal value of $(vk \pm \tilde{\omega})$, say k^* . Expanding the exponent to second order and replacing the function $\tilde{f}(k)$ by $\tilde{f}(k^*)$ yields a solvable Gaussian integral. A more detailed discussion can be found in Appendix B.

In this approximation, $\tilde{\mathcal{C}}^t$ will contain the constant terms from \mathcal{U}_1 and terms proportional to $t^{-1/2}$ that further oscillate both in space and in time. In their full extent, these terms are too complex to write down here but are easily used to compute numerical values for specific initial conditions. The supplementary Mathematica notebook contains an applet that shows the approximation for interactive initial conditions [22].

Figure 3 shows the PDF for a specific initial condition as a function of the site index n for a fixed time t . To show the quality of the approximation, we also show the relative difference

$$\varepsilon_r = \frac{2|p_s(n, t) - p_a(n, t)|}{p_s(n, t) + p_a(n, t)} \quad (18)$$

between the simulation p_s and the asymptotic expression p_a . Note that prediction and simulation are indistinguishable on this scale. The quality of the prediction remains excellent for general (complex and asymmetric) initial conditions $|\psi_0^0\rangle$.

The approximation can also be used for a fixed n as a function of t , as demonstrated in Fig. 4 for the initial site. The plot displays a short sequence of a time series at large t . Again, simulation and asymptotic approximation are indistinguishable on this scale.

To better understand the quality of the approximation, we plot the relative difference in the bottom part of Fig. 4. The data suggest, surprisingly, that the error of the approximation decays as $\sim t^{-3/2}$. This would imply that the method of stationary phase correctly predicts the leading behavior to order t^{-1} . This cannot be expected *a priori*, because the next order, obtainable with the method of steepest descent, may

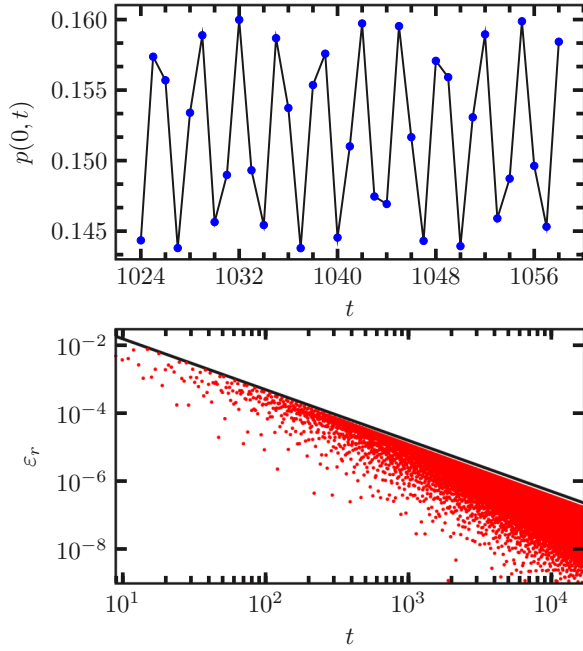


FIG. 4. (Color online) Top: A short time series of the probability at the initial site. The numerical values (blue circles) and the asymptotic approximation (black line) are indistinguishable on this scale. Bottom: The relative difference for $p(0,t)$ between the simulation and asymptotic approximation. The black line corresponds to $\sim t^{-3/2}$ and is only a guide to the eye.

yield terms of that order for \tilde{C}^t . Those should generate terms of the same magnitude in the PDF due to the constant eigenvalue. The data here suggest that such terms cancel out.

IV. WEAK LIMIT DISTRIBUTION

In the previous section, we found that the method of stationary phase yields a good approximation to the evolution of the quantum walk for sufficiently large times. It also became obvious that the PDF oscillates as a function of both n and t , especially close to the moving front, near $|v| \lesssim 1/\sqrt{3}$. In this section, we find a smooth approximation known as the weak limit [24]. We demonstrate that it yields a proper PDF, study the convergence toward it, and show that the walk spreads ballistically for all initial conditions.

A. Properties and implications

Following Ambainis *et al.* [10], we can separate out the rapidly oscillating part of Eq. (9). If we ignore the localized part for a moment, the corresponding distribution, which we will call $p_{\text{avg}}(n,t)$, can be found via

$$p_{\text{avg}}(n,t) = \langle \psi_0^0 | (\mathcal{U}_2^\dagger \mathcal{U}_2 + \mathcal{U}_3^\dagger \mathcal{U}_3) | \psi_0^0 \rangle. \quad (19)$$

This expression seems *ad hoc* but contains all nonoscillating terms from the full approximation. This corresponds to a temporal average at a specific site, assuming that the rapidly oscillating phase factors lead to a negligible contribution to the inverse Fourier transform (according to Riemann-Lebesgue). We argue that this also corresponds to a local spatial average at the

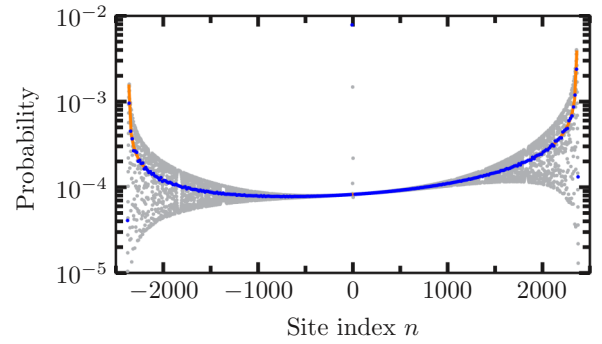


FIG. 5. (Color online) The smooth approximation p_{avg} from Eq. (19) (orange line) and the spatial average over 16 sites (blue dots) after 4096 time steps. The initial conditions are the same as in Fig. 3. The actual PDF is shown by gray dots.

fixed t , because as $t \rightarrow \infty$ a small change in n will only lead to a small change in v , such that the nonoscillating contribution should be the same in a neighborhood around a point that is reasonably small compared to t . This average also smoothes out the spatial oscillations of the PDF. In fact, we will use a spatial average to numerically predict p_{avg} .

Inserting the expressions for $\mathcal{U}_{2,3}(n,t)$, we find the matrix

$$\begin{aligned} \mathcal{U}_2^\dagger \mathcal{U}_2 + \mathcal{U}_3^\dagger \mathcal{U}_3 &= \frac{1}{\pi t \sqrt{2(1-3v^2)}(1-v^2)} \\ &\times \begin{bmatrix} (1-v)^2 & 2v(1-v) & 1-5v^2 \\ 2v(1-v) & 2-2v^2 & -2v(1+v) \\ 1-5v^2 & -2v(1+v) & (1+v)^2 \end{bmatrix} \end{aligned} \quad (20)$$

valid for all n subjected to $|n|/t < 1/\sqrt{3}$. Outside this interval, $p_{\text{avg}}(n,t) \equiv 0$. The dependency on n is implicit through $v = n/t$. For a specific initial condition, a comparison between the numerical simulation and the analytic prediction can be found in Fig. 5.

Our definition of $p_{\text{avg}}(n,t)$ closely relates to the weak limit proven by Grimmett *et al.* [24]. Note that $p_{\text{avg}}(n,t)/t$ only depends on v , which corresponds to $f(y)$ in their notation. They show that every quantum walk on regular lattices exhibits this convergence [for example, see Eq. (20) in [24]].

In the long-time limit, we can treat $v = n/t$ as a continuous variable. Hence, we approximate probabilities

$$p(n_- \leq n \leq n_+, t) = \sum_{n=n_-}^{n_+} p(n,t)$$

by integrals of the form

$$p(a \leq v \leq b, t) = \int_a^b p_{\text{avg}}(vt, t) t dv.$$

Here $a = n_-/t$ and $b = n_+/t$. By using the convergence of $p_{\text{avg}}(vt, t)$ to a stationary distribution solely depending on v , we conclude that the spreading is always ballistic. In this continuous limit, the localized part remains concentrated at the

initial site and

$$p_1(vt)t \rightarrow \langle \psi_0^0 | \begin{pmatrix} \frac{1}{\sqrt{6}} & 1 - \sqrt{\frac{2}{3}} & 2 - \frac{5}{\sqrt{6}} \\ 1 - \sqrt{\frac{2}{3}} & 1 - \sqrt{\frac{2}{3}} & 1 - \sqrt{\frac{2}{3}} \\ 2 - \frac{5}{\sqrt{6}} & 1 - \sqrt{\frac{2}{3}} & \frac{1}{\sqrt{6}} \end{pmatrix} | \psi_0^0 \rangle \delta(v), \quad (21)$$

characterizing the localization within the weak limit. Some algebra reveals that

$$\sum_{n=-\infty}^{\infty} p_1(n) + \int_{-1/\sqrt{3}}^{1/\sqrt{3}} p_{\text{avg}}(vt, t) t dv = 1, \quad (22)$$

i.e., our approximation actually yields a proper PDF. Connecting once more with [19], if the system starts in one of the three initial states (1, 0, 0), (0, 1, 0), and (0, 0, 1) each with probability 1/3, we rediscover

$$p(v, t) \approx \frac{1}{3} \delta(v) + \frac{4}{3\pi(1-v^2)\sqrt{2-6v^2}}.$$

However, observe that generically the numerator of the second term is quadratic in v rather than just a constant, as can be seen from Eq. (20). As an example, we utilize $p_{\text{avg}}(n, t)$ to approximate the second moment of the PDF. Figure 6 shows a comparison between the approximation and numerical simulations. The details of the calculation are in Appendix C, but the main result is that the second moment always grows $\sim t^2$ regardless of the initial conditions [see Eq. (C3)]. This means that only the PDF's shape can be influenced by $|\psi_0^0\rangle$, but not the asymptotic scaling of its spread.

In principle, we can approximate every moment, but the quality declines for higher moments. Those depend more strongly on sites farther away from the initial site where the accuracy is worse.

B. Convergence

In the previous sections, we have shown that the three-state quantum walk on the line is well described by a time-independent localized part and a ballistically moving front that can be approximated by a smooth PDF. In this section, we investigate how quickly the error of this approximation decays with time.

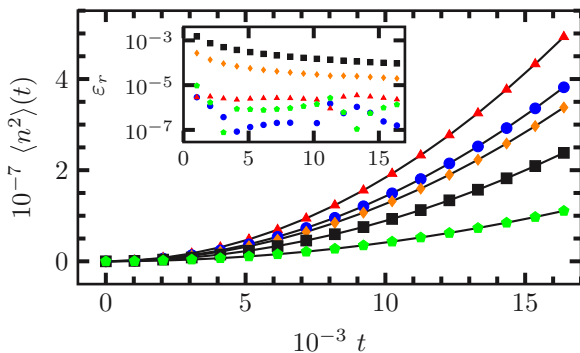


FIG. 6. (Color online) Comparison between the numerical values (symbols) and the evaluation of Eq. (C3) for the second moment of the PDF. Inset: The relative difference between the two values.

From the method of stationary phase, we already identified that the localization originates from the $\mathcal{U}_1^\dagger \mathcal{U}_1$ term, whereas p_{avg} stems from $\mathcal{U}_2^\dagger \mathcal{U}_2 + \mathcal{U}_3^\dagger \mathcal{U}_3$. We group the missing terms of the approximation into two functions:

$$q_1 = \langle \psi_0^0 | \mathcal{U}_1^\dagger (\mathcal{U}_2 + \mathcal{U}_3) + (\mathcal{U}_2 + \mathcal{U}_3)^\dagger \mathcal{U}_1 | \psi_0^0 \rangle, \quad (23)$$

$$q_{\text{avg}} = \langle \psi_0^0 | \mathcal{U}_2^\dagger \mathcal{U}_3 + \mathcal{U}_3^\dagger \mathcal{U}_2 | \psi_0^0 \rangle. \quad (24)$$

These functions are not non-negative quantities and hence cannot be interpreted as probabilities. In fact, both functions oscillate and average to zero. As Grimmet *et al.* [24] already pointed out, the convergence to the smooth probability function depends in general on the initial conditions. With our approximation, we can determine the slowest convergence rate.

From the formulas in the supplementary material [22], we see that the leading order of q_1 generically is $\sim t^{-1/2}$. By choosing special initial conditions, one can cancel this term and achieve a faster convergence $\sim t^{-3/2}$. This term dominates for small n but is exponentially suppressed for large n . In that case $q_{\text{avg}} \gg q_1$ and a different convergence rate is possible. In fact, for $n \gg 1$, the deviation from the smooth PDF decay is at least $\sim t^{-3}$, for particular initial conditions even $\sim t^{-5}$.

Figure 7 illustrates our findings. It shows the convergence toward $p_1(0) + p_{\text{avg}}(0, t)$ for two different initial conditions at two different sites. The smooth PDF is represented by the orange line. The envelopes (black lines) are derived from Eqs. (23) and (24) depending on the site.

Our calculations enable us to make statements about the convergence of the PDF toward the limiting distribution. We have already seen that the oscillations around the stationary value at the initial site decay $\sim t^{-1/2}$. This was due to the contribution of $\mathcal{U}_1(n)$. But for sites sufficiently far away from the initial site, this term becomes exponentially small, and the asymptotic behavior changes. The right panels of Fig. 7 present data similarly to the left, but for $n = 512$. By changing the x axis to t^{-1} , it is evident from the inset that $p(512, t) \sim t^{-1}$ for sufficiently large times. This corresponds to the stationary distribution itself. By computing the envelope, we find that the next order correction vanishes $\sim t^{-3}$, resulting in a correction $O(t^{-2})$ for the stationary distribution.

V. CONCLUSION

We studied the three-state quantum walk on the line in the long-time limit using the method of stationary phase. We found explicit formulas for the localization that are asymmetric around the initial site. The degree of asymmetry, including the extreme cases where the localization vanishes completely either for positive or negative site indices, solely depends on the initial conditions (see Fig. 2). We showed how the weak limit of the PDF can be interpreted as a time average at a fixed site, or as a spatial average for a fixed t . We used the latter interpretation to demonstrate the good agreement between the asymptotic approximation and long-time simulations. We applied the smooth, approximative PDF to show that the quantum walk always spreads ballistically for all initial conditions. Finally, we studied the convergence toward this smooth description. We identified the generic convergence rate depending on the

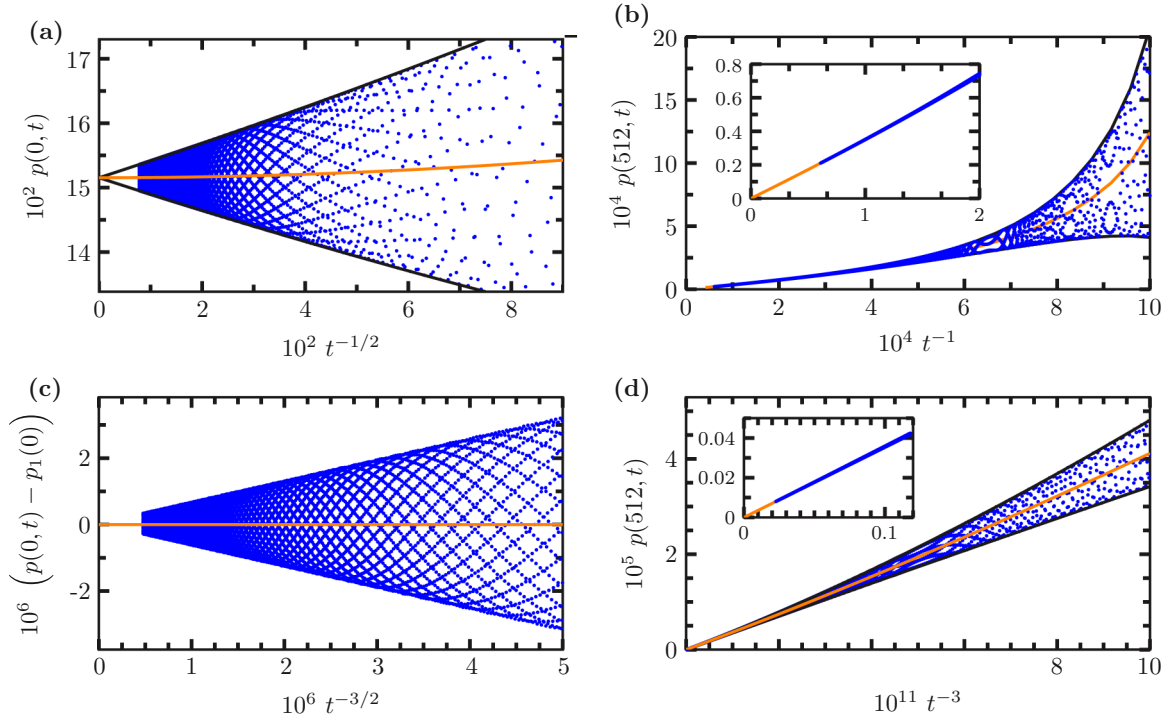


FIG. 7. (Color online) The numerically observed probabilities (blue dots), the weak limit approximation $p_1(n) + p_{\text{avg}}$ (orange line), and the corresponding envelopes from the long-time approximation (black lines). For the upper panels, it is $|\psi_0^0\rangle \propto (0, i, 1)^T$; for the lower ones, it is $|\psi_0^0\rangle \propto (1, 0, -1)^T$. The left panels refer to the initial site, whereas the right ones refer to $n = 512$, to contrast sites with and without significant localization. Note the difference in scaling with time, depending on the initial conditions. Inset: Zoom for large times on the same t scale. For the data in panel (c), there is no prediction from the method of stationary phase, because for $n = 0$ all available orders cancel. However, from the formulas we know that the envelope should scale $\sim t^{-3/2}$, as supported by the numerical data.

site index and pointed out that other initial conditions only converge faster.

ACKNOWLEDGMENTS

We gratefully acknowledge helpful discussions with R. Portugal. This work was supported by Division of Materials Research Grant No. 1207431 from the NSF.

APPENDIX A: THE STATIONARY PROBABILITY DISTRIBUTION

The nontrivial limit of the PDF as $t \rightarrow \infty$ is purely determined by the κ -independent eigenvalue of \tilde{C} in Eq. (7). To find this “stationary state,” we evaluate the definition of \mathcal{U}_1 in Eq. (11). For this calculation, we do not have to resort to any approximation but can solve the integrals analytically by applying the residue theorem. As already mentioned in the text, all components share the two poles

$$\kappa_{\pm} = -5 \pm 2\sqrt{6},$$

of which only κ_+ lies inside the unit circle. Depending on n , there is an additional pole at $\kappa = 0$. After some simple algebra,

we find

$$\begin{aligned} \mathcal{U}_1(n) = & \kappa_+^n \begin{bmatrix} \frac{1}{\sqrt{6}} & 1 - \sqrt{\frac{2}{3}} & 2 - \frac{5}{\sqrt{6}} \\ -1 - \sqrt{\frac{2}{3}} & -\sqrt{\frac{2}{3}} & 1 - \sqrt{\frac{2}{3}} \\ -2 - \frac{5}{\sqrt{6}} & -1 - \sqrt{\frac{2}{3}} & \frac{1}{\sqrt{6}} \end{bmatrix} \\ & + \text{Res}_{\kappa=0}(\kappa^{n-1} \tilde{\mathcal{M}}_1). \end{aligned} \quad (\text{A1})$$

Please refer to the supplementary material for the full expression of $\tilde{\mathcal{M}}_1$ [22]. The last term is only nonzero if $n \leq 0$ and counteracts the divergence of κ_+^n as $n \rightarrow -\infty$. All residues are of the form

$$\text{Res}_{\kappa=0} \left(\frac{a\kappa^m}{1 + 10\kappa + \kappa^2} \right).$$

To calculate the residue, note that with partial fractions

$$\begin{aligned} \frac{1}{1 + 10\kappa + \kappa^2} &= \frac{1}{4\sqrt{6}} \left[\frac{1}{\kappa_- - \kappa} - \frac{1}{\kappa_+ - \kappa} \right] \\ &= \frac{1}{4\sqrt{6}} \left[\sum_{k=0}^{\infty} \frac{\kappa^k}{\kappa_-^{k+1}} - \sum_{k=0}^{\infty} \frac{\kappa^k}{\kappa_+^{k+1}} \right]. \end{aligned}$$

With this representation, we find

$$\begin{aligned} \text{Res}_{\kappa=0} \left(\frac{a\kappa^m}{1+10\kappa+\kappa^2} \right) &= \frac{a}{2\pi i} \oint \kappa^m \frac{1}{1+10\kappa+\kappa^2} d\kappa \\ &= \frac{a}{4\sqrt{6}} \sum_{k=0}^{\infty} (\kappa_-^{-k-1} - \kappa_+^{-k-1}) \underbrace{\frac{1}{2\pi i} \oint \kappa^{m+k} d\kappa}_{=\delta_{-1,m+k}} \\ &= \frac{a}{4\sqrt{6}} [\kappa_-^m - \kappa_+^m]. \end{aligned}$$

Plugging this result into Eq. (A1) yields Eq. (13).

APPENDIX B: APPROXIMATION FOR LONG TIMES

The inverse Fourier transform reads

$$\begin{aligned} |\psi_n^t\rangle &= \left(\frac{1}{2\pi} \int_{-\pi}^{\pi} e^{ink} \tilde{C}^t dk \right) |\psi_0^0\rangle \\ &= [\mathcal{U}_1(n) + \mathcal{U}_2(n,t) + \mathcal{U}_3(n,t)] |\psi_0^0\rangle. \end{aligned}$$

We have already seen how $\mathcal{U}_1(n)$ emerges from the constant eigenvalue and how it can be calculated explicitly. For the evaluation of Eq. (16), we have to resort to an asymptotic analysis for $t \rightarrow \infty$. Note that the integrals can be written as

$$\frac{1}{2\pi} \int_{-\pi}^{\pi} f(k) e^{ink \pm it\tilde{\omega}} dk,$$

where $f(k)$ represents the components of $\tilde{\mathcal{M}}_{2,3}$. Before we can apply the method, we introduce the parameter v [see Eq. (17)]. This allows us to write the integrals in the form

$$\frac{1}{2\pi} \int_{-\pi}^{\pi} f(k) e^{it[vk \pm \omega(k)]} dk := \frac{1}{2\pi} \int_{-\pi}^{\pi} f(k) e^{it\rho(k)} dk.$$

The idea is now to expand $\rho(k)$ around any extrema k^* to second order:

$$\rho(k) = \rho(k^*) + \frac{1}{2} \rho''(k^*) (k - k^*)^2 + O((k - k^*)^3).$$

For $t \rightarrow \infty$, this captures the main contribution around these points of stationary phase, and everything else is exponentially suppressed. This requires $f(k^*) \neq 0$, which holds for all integrals considered here. Within this scheme the integral is approximated by

$$\int f(k) e^{it\rho(k)} dk \approx f(k^*) e^{it\rho(k^*)} \int e^{\frac{it\rho''(k^*)}{2} (k-k^*)^2} dk,$$

and the remaining Gaussian integral can be computed exactly. Caution has to be taken with the additional rotation by $\pi/4$ to transform the exponent into the real domain. The direction depends on the sign of $\rho''(k^*)$. This rotation turns the original integration path into a steepest descent where $|\rho''|$ varies the most.

The extrema occur at $k^* = \pm \arccos(\frac{1-5v^2}{v^2-1})$ depending on the eigenvalue at hand and the sign of v . There is always one such point for each eigenvalue. Furthermore, we find the

simple expression

$$\rho''(k^*) = \pm \frac{\sqrt{2}}{4} \sqrt{1-3v^2(1-v^2)}.$$

The expressions for $\tilde{\mathcal{M}}_{2,3}(k^*)$ can be found in the Mathematica file [22]. They still contain case distinctions for the sign of n , which disappear when calculating the expression for p_{avg} in Eq. (20).

APPENDIX C: CALCULATING MOMENTS

Assuming the $p_{\text{avg}}(n,t)$ is always a good approximation and that the localized part does not contribute to the time dependence of any moment, we calculate the first three moments of the PDF, $\langle n^k \rangle$ for $k = 0, 1, 2$. However, instead of performing sums over all n , we approximate them by integrals:

$$\begin{aligned} \langle f(n) \rangle &= \sum_{n=-\infty}^{\infty} f(n) p(n,t) \\ &\approx \int_{-1/\sqrt{3}}^{1/\sqrt{3}} f(vt) p_{\text{avg}}(vt,t) t dv. \end{aligned}$$

Applying this to every matrix entry in Eq. (20) yields

$$\langle n^0 \rangle = \frac{1}{\sqrt{6}} \langle \psi_0^0 | \begin{bmatrix} -1 + \sqrt{6} & 2 - \sqrt{6} & 5 - 2\sqrt{6} \\ 2 - \sqrt{6} & 2 & 2 - \sqrt{6} \\ 5 - 2\sqrt{6} & 2 - \sqrt{6} & -1 + \sqrt{6} \end{bmatrix} | \psi_0^0 \rangle, \quad (\text{C1})$$

$$\begin{aligned} \langle n \rangle &= \frac{t}{\sqrt{6}} \langle \psi_0^0 | \\ &\times \begin{bmatrix} 2 - \sqrt{6} & -2 + \sqrt{6} & 0 \\ -2 + \sqrt{6} & 0 & 2 - \sqrt{6} \\ 0 & 2 - \sqrt{6} & -2 + \sqrt{6} \end{bmatrix} | \psi_0^0 \rangle, \quad (\text{C2}) \end{aligned}$$

$$\begin{aligned} \langle n^2 \rangle &= \frac{t^2}{6\sqrt{6}} \langle \psi_0^0 | \\ &\times \begin{bmatrix} -13 + 6\sqrt{6} & 14 - 6\sqrt{6} & 29 - 12\sqrt{6} \\ 14 - 6\sqrt{6} & 2 & 14 - 6\sqrt{6} \\ 29 - 12\sqrt{6} & 14 - 6\sqrt{6} & -13 + 6\sqrt{6} \end{bmatrix} | \psi_0^0 \rangle. \quad (\text{C3}) \end{aligned}$$

We observe that the zeros moment is unity only for the initial conditions that show no localization, $\langle \psi_0^0 | \propto (1, -2, 1)^T$. The matrix for the first moment has the eigenvector $(1, 1, 1)^T$ with eigenvalue zero. However, this does not cover all symmetric initial conditions that will yield a zero first moment by symmetry. It easily verified that the initial conditions $\sim (1, 0, 1)^T$ also yield a zero first moment. Hence, every linear combination of those two will do so, too, which now covers all symmetric initial conditions. These asymptotic formulas show that any nonzero first moment grows linearly in time while the second moment is proportional to t^2 .

[1] J. Kempe, *Contemp. Phys.* **44**, 307 (2003).

[2] N. Konno, in *Quantum Potential Theory*, Lecture Notes in Mathematics Vol. 1954, edited by U. Franz and

M. Schürmann (Springer-Verlag, Heidelberg, 2008), pp. 309–452.

[3] S. E. Venegas-Andraca, *Quant. Info. Proc.* **11**, 1015 (2012).

- [4] R. Portugal, *Quantum Walks and Search Algorithms* (Springer, Berlin, 2013).
- [5] Y. Aharonov, L. Davidovich, and N. Zagury, *Phys. Rev. A* **48**, 1687 (1993).
- [6] D. A. Meyer, *J. Stat. Phys.* **85**, 551 (1996).
- [7] L. K. Grover, *Phys. Rev. Lett.* **79**, 325 (1997).
- [8] E. Farhi and S. Gutmann, *Phys. Rev. A* **58**, 915 (1998).
- [9] D. Aharonov, A. Ambainis, J. Kempe, and U. Vazirani, in *ACM Symposium on Theory of Computation (STOC'01)* (ACM, New York, 2001), pp. 50–59.
- [10] A. Ambainis, E. Bach, A. Nayak, A. Vishwanath, and J. Watrous, in *Proceedings of the Thirty-Third Annual ACM Symposium on Theory of Computing, STOC '01* (ACM, New York, 2001), pp. 37–49.
- [11] E. Bach, S. Coppersmith, M. P. Goldschen, R. Joynt, and J. Watrous, *J. Comput. Syst. Sci.* **69**, 562 (2004).
- [12] A. M. Childs and J. Goldstone, *Phys. Rev. A* **70**, 022314 (2004).
- [13] A. Ambainis, *Int. J. Quantum. Inform.* **01**, 507 (2003).
- [14] K. Rudinger, J. K. Gamble, E. Bach, M. Friesen, R. Joynt, and S. N. Coppersmith, *Journal of Computational and Theoretical Nanoscience* **10**, 1653 (2013).
- [15] A. M. Childs, *Phys. Rev. Lett.* **102**, 180501 (2009).
- [16] N. B. Lovett, S. Cooper, M. Everitt, M. Trevers, and V. Kendon, *Phys. Rev. A* **81**, 042330 (2010).
- [17] M. C. Bañuls, C. Navarrete, A. Pérez, E. Roldán, and J. C. Soriano, *Phys. Rev. A* **73**, 062304 (2006).
- [18] Y. Shikano and H. Katsura, *Phys. Rev. E* **82**, 031122 (2010).
- [19] N. Inui, N. Konno, and E. Segawa, *Phys. Rev. E* **72**, 056112 (2005).
- [20] N. Inui, Y. Konishi, and N. Konno, *Phys. Rev. A* **69**, 052323 (2004).
- [21] S. Boettcher, S. Falkner, and R. Portugal, [arXiv:1311.3369](https://arxiv.org/abs/1311.3369).
- [22] See Supplemental Material at <http://link.aps.org/supplemental/10.1103/PhysRevA.90.012307> for detailed formulas and interactive plots for different initial conditions.
- [23] C. M. Bender and S. A. Orszag, *Advanced Mathematical Methods for Scientists and Engineers: Asymptotic Methods and Perturbation Theory* (Springer, New York, 1999), Vol. 1.
- [24] G. Grimmett, S. Janson, and P. F. Scudo, *Phys. Rev. E* **69**, 026119 (2004).